



Analysis of urban-scale typhoon precipitation characteristics and spatiotemporal patterns: A case study of Ningbo, China

Caiming Wu^{1,2} Yi Lu^{3,4} Hong-Li Ren² Fumin Ren²

¹Collaborative Innovation Center on Forecast and Evaluation of Meteorological Disasters (CIC-FEMD), School of Atmospheric Science, Nanjing University of Information Science and Technology, Nanjing, 210044, China;

²State Key Laboratory of Severe Weather Meteorological Science and Technology, and Center for Meteorological Impact and Risk Research, Chinese Academy of Meteorological Sciences, Beijing, 100081, China;

³Shanghai Typhoon Institute, China Meteorological Administration, Shanghai, 200030, China;

⁴Asia-Pacific Typhoon Collaborative Research Center, Shanghai, 200030, China.

10 *Correspondence to:* Yi Lu (luy@typhoon.org.cn); Fumin Ren (fmren@163.com)

Abstract. Rainstorm characterization, which is the fundamental design basis for urban flood control and drainage systems, currently relies primarily on general statistical regularities of heavy rainfall. The current design rainstorm profile (e.g., Chicago hyetograph) overlooks the spatial non-uniformity and unique intensity–duration–frequency (IDF) relationships of typhoon rainfall. This deficiency constitutes a key reason for the systemic failure of urban flood defence engineering when facing extreme typhoon rainfall events. To address this problem, the current study focused on the area of Ningbo in China. Using meteorological station observations, county-level IDF curves for annual maximum typhoon rainfall at specific durations were established, and then the K-means clustering method was applied to extract typical spatiotemporal patterns of typhoon rainfall, which produced the following results. The impact of typhoons in the Ningbo area manifests primarily as extreme rainfall of long duration, with 24-h rainfall being the most notable contributor. Current published IDF curves underestimate the extremes for such prolonged typhoon-related events. Owing to the spatial non-uniformity of typhoon rainfall, marked regional variations of IDF curves are observed across county-level areas. Furthermore, typhoon impacts, as revealed by extension of the study period from 1980–2014 to 1980–2024, exhibited spatially inhomogeneous enhancement, with notable increase in the northern region, reflected primarily in the frequency of extreme events. The extracted temporal rainfall patterns for typhoon events are dominated by the central-peaked pattern (with rainfall concentrated in the middle phase) and the late-peaked pattern, differing substantially from the Chicago hyetograph. The latter exhibits limitations in characterizing the structure of long-duration typhoon-related rainfall because it tends to overestimate peak rainfall intensity. Spatially, rainfall patterns are categorized into dispersed-dominated and concentrated types. Topography is the key driver of local rainfall patterns, dictating the spatial loci and temporal windows in which heavy rainfall develops and suddenly intensifies. Typhoons and their interactions with other weather systems also enhance the local specificity of rainfall patterns. These insights could help in designing realistic typhoon rainfall scenarios for urban flood defence planning.



1 Introduction

Typhoons (i.e., tropical cyclones), through secondary flooding triggered by torrential rainfall, remain one of the world's most destructive natural hazards. In both Typhoon Helene (2024) in North Carolina, USA, and Typhoon Kalmaegi (2025) in Cebu, Philippines, heavy casualties resulted primarily from severe flooding triggered by the extreme rainfall. In coastal
35 China, typhoons are the primary weather system responsible for extreme precipitation events (Zhang et al., 2018), which often result in flooding (Su et al., 2015; Xu et al., 2022; Wang et al., 2025). During Typhoon Fitow in 2013, record rainfall flooded 70% of Yuyao City in Zhejiang Province (China), with the core urban area experiencing 90% inundation. Water level at the Yao River's Yuyao station peaked at 3.46 m, surpassing previous records (Chan et al., 2022). Typhoon Lekima
40 (2019) remained over mainland China for more than 44 h, causing varying degrees of urban and rural waterlogging and river flooding across multiple provinces (Xu et al., 2022; Zhou et al., 2022), and inundating entirely Linhai City in Zhejiang Province (Zhou et al., 2022). In 2021, Typhoon In-Fa moved slowly and exerted prolonged influence on parts of China, with continuous rainfall persisting for seven days, resulting in exceptionally high cumulative precipitation. The water level at Yuyao station reached a new record height of 3.53 m. Despite notable upgrades and effective operation of flood defence
45 systems (Chan et al., 2022), drainage and flood control infrastructure still faced immense pressure under the scenarios outlined above. Studies over recent years also indicate that the occurrence of typhoon-induced heavy rainfall is increasing (Kossin, 2018; Li, 2020; Emanuel, 2017; Liu et al., 2020), and the risk of secondary flooding is projected to rise correspondingly.

For purposes such as designing flood control and drainage infrastructure, quantitatively assessing rainstorm disaster risk, and addressing the impact of climate change, a fundamental task is to understand and scientifically characterize regional rainfall
50 features (Lanciotti et al., 2022). Through quantification of extreme rainfall intensity over specific durations and recurrence periods, and analysis of the spatiotemporal structure of heavy rainfall, the statistical characteristics of extreme precipitation can be transformed into physical inputs that drive flooding response simulations and dynamic risk management.

Intensity–duration–frequency (IDF) curves are an internationally recognized core tool for urban drainage design, flood risk analysis, and water resource engineering planning. In the United States, NOAA's Office of Hydrology developed a national,
55 standardized system providing site-specific IDF data across varying durations (5 min to 60 days) and return periods (1–1,000 years) using statistical and regional analysis methods (Hosking, 1990; Lin et al., 2006). Through the point-to-surface conversion method, single-point IDF curves can be scaled to the catchment level (Sivapalan and Blöschl, 1998; MLIT, 2015; MLIT and NILIM, 2023). In recent years, global high-resolution IDF datasets such as BURGER (Hoch et al., 2025) have been successively released. Non-stationary IDF analysis under the impact of climate change is also gaining global attention
60 (Lima et al., 2016; Cannon et al., 2019; Jayaweera et al., 2025). In China, despite considerable progress in developing short-duration IDF curves (Ren et al., 2025), the fragmented governance between urban drainage (short duration) and river flood control (long duration) has weakened system resilience against extreme rainfall events (Zhou et al., 2022). In contrast,



research in China on IDF curves that comprehensively consider both long and short durations started relatively late and has been conducted primarily on a localized, region-by-region basis.

65 Traditional rainfall pattern analysis often assumes a spatially uniform distribution or relies on coarse zoning, while focusing on the temporal rainfall profile within a region. Zhang et al. (2021) summarized seven representative profiles. Common design rainfall profile methods include, for short-duration events, the Chicago hyetograph, Huff hyetograph, triangular hyetograph, and Pilgrim and Cordery hyetograph. For long-duration events, common methods include the Soil Conservation Service hyetograph (Soil Conservation Service, 1986) and the same-frequency amplification analysis method (Yan et al.,

70 2020). Among these, the Chicago hyetograph and the same-frequency amplification analysis method (Li et al., 2024) are the ones used most widely for short- and long-duration rainfall, respectively. In practice, the Chicago hyetograph is often applied alone or integrated with the latter for long-duration events. To enhance the realism and engineering applicability of design scenarios, Yang et al. (2024) extracted representative temporal rainfall patterns from historical rainfall events through intelligent clustering and similarity assessment. Additionally, Qi et al. (2022) examined the impact of different rainfall

75 patterns on flooding, finding that the single-peak pattern might lead to more severe results. As high-resolution observational data continue to accumulate and diversify, recent studies indicate that the spatial distribution characteristics of rainfall are key factors determining flooding characteristics (Costabile et al., 2023; Xu et al., 2025). Spatial non-uniformity of rainfall increases urban flooding areas and water volumes, altering the spatial distribution patterns of flooding (Chen et al., 2022; Lin et al., 2022).

80 The prolonged duration, massive cumulative rainfall, and extensive coverage of typhoon-related rainstorms shape their unique disaster-causing mechanisms. These characteristics make them more prone to triggering severe, urban-scale, and systemic urban flooding. Existing research, however, has overlooked these critical characteristics of heavy rainfall associated with such specific weather systems. Meanwhile, Ji et al. (2025) analysed hourly scale heavy rainfall events from landfalling typhoons in China. They found that events persisting for more than 12 h accounted for the highest proportion (39.93%) and

85 showed a substantial annual increase of 0.13%. The average annual duration reached 19.93 h and continued to lengthen by 0.03 h annually. Short-duration events (1–6 h) accounted for the lowest proportion (29.79%) but the fastest growth rate (0.17% annually), while their duration showed slight decrease.

It is evident that research on urban storm characteristics and flood control strategies urgently requires greater focus on typhoon-induced precipitation, particularly the long-duration heavy rainfall events such systems generate. The outcomes of

90 IDF curves are applied predominantly in the design of temporal rainfall patterns, while spatial variability is often addressed by zoning IDF curves based on regional rainfall characteristics. For temporal rainfall patterns, long-duration designs are sometimes oversimplified through mechanistic extension of short-duration design rainfall patterns, leading to distorted rainfall distributions; in other cases, reliance on a limited number of typical historical storm events restricts flexibility and generalizability. Spatial rainfall patterns mostly lack a universally applicable theoretical framework or standardized

95 analytical methods. The scarcity and/or inaccessibility of high-resolution, long-term rainfall data have largely confined



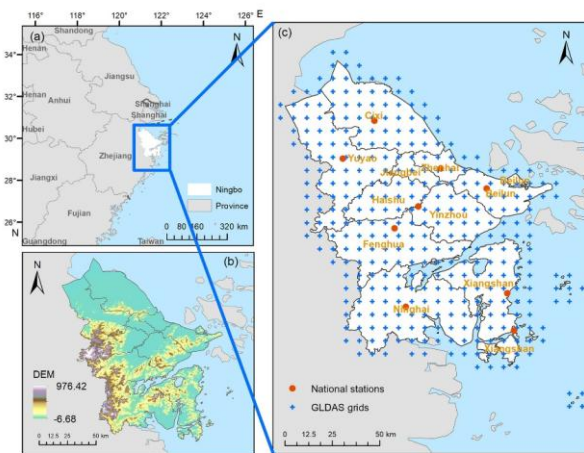
research on spatial rainfall patterns to hypothetical scenarios, resulting in incomplete understanding of their physical characteristics.

This study selected Ningbo, a representative typhoon-affected city in China, to specifically investigate the IDF characteristics and key spatiotemporal rainfall patterns of typhoon rainstorms. The remainder of this paper is structured as follows. Section 2 introduces the study area and the data and methods used. Section 3 discusses the research findings, and Section 4 presents the derived conclusions and outlines further prospects.

2 Data and methodology

2.1 Study area

Ningbo, a sub-provincial city in Zhejiang Province, China (Fig. 1a), covers a land area of 9,816 km², has a population of 9.78 million, and produced a GDP value of 1,814.77 billion RMB in 2024. It is located on the southern wing of the Yangtze River Delta (28°51'–30°33'N, 120°55'–122°16'E), bordered by the East China Sea to the east and Hangzhou Bay to the north. The region is characterized by varied topography that includes northeastern plains and southwestern hills (Fig. 1b). Ningbo has a dense network of rivers, including the Yongjiang River, one of Zhejiang Province's eight major water systems. The Yuyao River and Fenghua River converge within the urban area, flowing north-eastward into the East China Sea. Ningbo experiences a subtropical monsoon climate with average annual rainfall of 1,539 mm. Rainfall is concentrated from May to September, mainly during the monsoon and typhoon seasons. As one of the regions in China most frequently and severely affected by tropical cyclones, Ningbo has experienced multiple severe urban flood events triggered by typhoons (e.g., Haikui in 2012, Fitow in 2013, In-Fa in 2021, and Muifa in 2022). Observations reveal substantial spatiotemporal variability in typhoon-related rainfall, making Ningbo an ideal study area.



115

Figure 1: Overview of the study area. (a) Location of the study area, (b) the regional topography, and (c) the locations of national meteorological stations and the coverage of the China Meteorological Administration Land Data Assimilation System (CLDAS) grid. Base map of China: GS (2024) 0650.



2.2 Data

120 2.2.1 Basic data

(1) Historical TC data were acquired from the best-track dataset maintained by the Shanghai Typhoon Institute of the China Meteorological Administration (CMA). This dataset has been quality-controlled and is recorded in Coordinated Universal Time (UTC) (Ying et al., 2014; Lu et al., 2021).

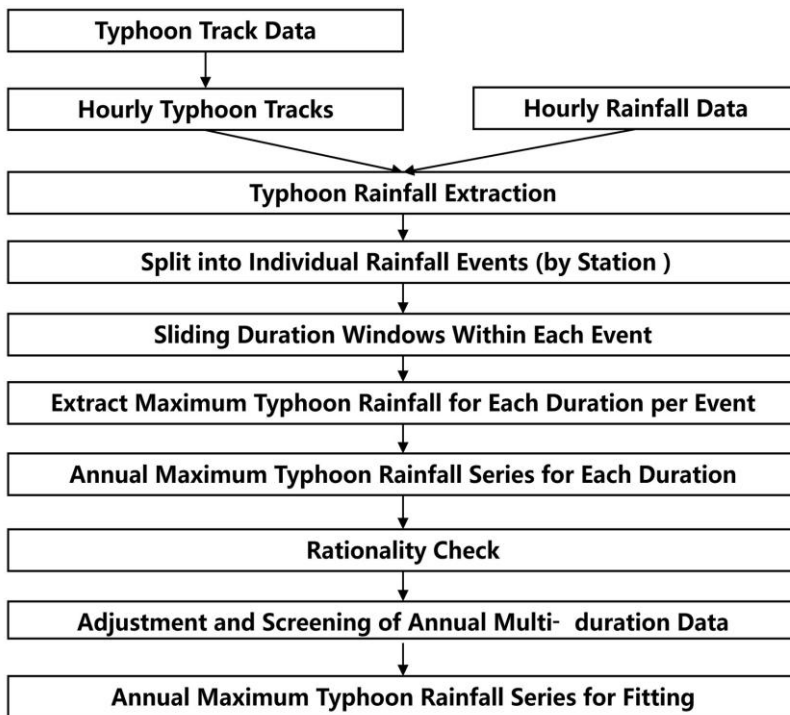
125 (2) Hourly precipitation data (Zhao et al., 2024) from 1951 to present for nine national stations in Ningbo (Fig. 1c) were extracted from the National Meteorological Information Center of the CMA. Yinzhou station was considered representative of the urban centre. Data from Zhenhai station were excluded because of missing records, and Shipu station was generally not considered. This dataset has undergone quality control and is recorded in Beijing Time (BJT).

(3) Gridded precipitation data were sourced from the CMA Land Data Assimilation System (CLDAS) hourly product (Sun et al., 2020). This dataset integrates ground observations, satellite remote sensing, and numerical model data. The data have
130 been quality-controlled and have spatial resolution of 0.0625° . This dataset is recorded in UTC, starting from 1 January 1998, 00:00:00.

(4) The Forest And Buildings removed Copernicus DEM (FABDEM), developed jointly by the company Fathom (UK) and the University of Bristol (UK), is the first global digital elevation model (DEM) with forest and buildings removed presented at 30-m resolution. It is currently one of the most accurate free digital elevation datasets worldwide, with a mean absolute
135 vertical error of 1.12 and 2.88 m globally and in forested areas, respectively (Hawker et al., 2022).

2.2.2 Preprocessing of typhoon track and hourly precipitation data

First, meteorological data required preprocessing (Fig. 2). This involved interpolation of typhoon track data, hourly precipitation separation of typhoons, and division of typhoon rainfall processes. The track locations of each typhoon were first interpolated to hourly resolution, and the area impacted directly by rainfall was then defined as being within 500 km of
140 the typhoon location at each time step. To define rainfall processes, for each typhoon, single-station rainfall data were first sorted chronologically. Then, a rainfall event (or process) was defined as beginning when rainfall exceeded 0.1 mm/h, and ending at the time of the final occurrence of measurable rainfall of more than 0 mm/h that was followed immediately by two or more consecutive hours of zero rainfall. The next event was defined as beginning at the first instance of rainfall exceeding 0.1 mm/h after the previous event had ended, and the process continued in this manner (Zhang, 2015; Tang et al., 2020).



145

Figure 2: Flowchart for extracting annual maximum typhoon rainfall series at specific durations for each station.

For sample selection in curve fitting, each station was processed independently. Within each rainfall event, a sliding window was moved with a time step of 1 h to compute the cumulative rainfall for window lengths of 1, 3, 6, 9, 12, 15, 18, 24, 36, and 48 h. For each window length, the event-specific maximum rainfall was determined by sorting and comparing the computed values. When identifying the annual maximum typhoon rainfall, the selected rainfall process for a given duration was not constrained by day or month boundaries, provided it did not cross year boundaries. For each duration (i.e., window length), the annual maximum was then determined by further comparing these event-specific maxima across all events within a year. During the rationality check (Fig. 2), it was found that when rainfall events (or processes) were divided according to the above criteria, some typhoon influence processes might have been excessively segmented. This could have led to two issues: (1) annual maximum rainfall for longer durations being lower than that for shorter durations in the same year, and (2) insufficient valid samples for longer durations. The segmentation was adjusted to a typhoon-influence process when the first issue occurred. For each typhoon, single-station rainfall data were also first sorted chronologically. Then, a typhoon-influence process was defined as each continuous period during which the station remained within a 500-km radius of the typhoon location. Unlike the rainfall-event definition, which required specific rainfall intensity thresholds to initiate or terminate an event, this broader definition captured the entire duration of the direct influence of the typhoon. Consequently, a single typhoon might have included multiple such processes if the station intermittently entered and exited the 500-km range.

150

155

160



After optimizing the process segmentation, the rationality of the data was improved substantially and the occurrence of the second issue was alleviated accordingly.

165 The first issue rarely persisted after the above adjustments. If it did, to ensure that no extreme values were missed, the hourly series corresponding to the short-duration maxima was extended to longer durations. For the year in which the issue was identified, the maximum rainfall value across all durations shorter than the target duration was extracted. Zeros were then prepended to the corresponding rainfall series, based on historical experience that a more hazardous rainfall peak usually occurs later. Then, the cumulative rainfall over this extended series was used to replace the original annual maximum rainfall for the longer duration.

170 Annual sequence data for fitting were further screened to define impactful rainfall events (Fig. 2), with thresholds from the “*Precipitation Classification Standard*” (GB/T 28592-2012): 12-h rainfall ≥ 15 mm or 24-h rainfall ≥ 25 mm, depending on the longest duration in the given year. The selection of these thresholds could also balance the sample size requirements for fitting.

2.3 Method

175 2.3.1 Fitting IDF curves based on annual maximum typhoon rainfall series

The empirical frequency was calculated using the mathematical expectation formula recommended by the “*Technical Guidelines for Establishment of Intensity–Duration–Frequency Curve and Design Rainstorm Profile*,” issued jointly by the Ministry of Housing and Urban–Rural Development of the People’s Republic of China and the CMA. The formula is expressed as follows:

$$180 \quad P = \frac{m}{n+1} \times 100\%, \quad (1)$$

where P is the empirical frequency and n is the total number of samples. The samples are arranged in descending order as x_1, x_2, \dots, x_n . For a given sample, its rank m is defined as the count of occurrences greater than or equal to that sample.

185 The Pearson-III, Generalized Extreme Value distribution, Gumbel distribution, and Exponential distribution were selected for consideration, all of which are commonly used distributions in extreme value analysis (Ghanmi et al, 2016; Gruss et al, 2025). Curve fitting, which seeks the best agreement between the frequency curve and the empirical data, was performed using a combined approach of objective fitting and optimized fitting methods. The key to curve fitting is the criterion used to measure the best agreement. This study considered three fitting criteria: the minimum sum of the squared deviations, the minimum sum of the absolute deviations, and the minimum sum of the squares of the relative deviations.

190 Based on the fitting results, the curve fitting scheme was adjusted primarily to address the issue of intersecting fitted curves for different durations at the same station. This study adopted a variable ratio of the coefficient of skewness (C_s) to the coefficient of variation (C_v), using three strategies. The first strategy was to calculate the average ratio based on all durations at the station and set it as the standard value with an allowable error range of ± 0.6 , while setting some initial parameters of



the fitting function based on the characteristics of the observed data (such as mean and variance). Second, the optimal parameters obtained for a given duration were used sequentially as the initial parameters for fitting the curve of the immediately longer duration. Finally, based on the intrinsic characteristics of the distribution functions, parameters were adjusted within a reasonable range. In this strategy, the constraint on the allowable error margin for the ratio was relaxed and thus the fitting error itself served as the primary control criterion.

For error validation, with reference to the technical guidelines mentioned above, when the return period was between 2 and 20 years, the mean absolute root mean square error (RMSE) should not exceed 0.05 mm/min in areas with moderate rainfall intensity, whereas in areas with higher rainfall intensity, the mean relative root mean square error (MRRMSE) should not exceed 5%. These two metrics can be expressed as follows:

$$RMSE = \sqrt{\frac{1}{n} \sum_{i=1}^n \left(\frac{R'_i - R_i}{t_i} \right)^2}, \tag{2}$$

$$MRRMSE = \sqrt{\frac{1}{n} \sum_{i=1}^n \left(\frac{R'_i - R_i}{R_i} \right)^2} \times 100\%, \tag{3}$$

where R'_i is the theoretical rainfall amount, R_i is the rainfall amount determined from the fitting values, t_i is the rainfall duration, and n is the number of samples. Meanwhile, reference was made to Appendix C of the “*Ningbo Urban Drainage and Waterlogging Control Detailed Rules*” (Yong DX/JS 021-2023) and to the “*Standard of rainfall intensity computation*” (DB33/T 1191-2020). The fitted values were compared with results inversely calculated from formulas provided in the reference materials (Table 1). Additionally, graphical checks were conducted to examine whether the multi-duration IDF curves exhibited intersections under each combination of fitting functions and criteria for each station.

Table 1: Comparison of data sources and methods for IDF curves from different origins.

IDF curves from DB33/T 1191-2020 and Yong DX/JS 021-2023 (durations: 5–180 min; return periods: 1–100 yr)					IDF curves in this study
County	IDF Curves (Rainstorm Intensity Formula)	Data Period & Duration	Selection Method /Theoretical Distribution	Station and level	
Ningbo Main Urban	$q = \frac{6576.744 \times (1 + 0.685 \lg P)}{(t + 25.309)^{0.921}}$	1981–2014 (34 years)	Annual maximum rainfall series for	Yinzhou National	• Comparison: 1980–2014 (35)



IDF curves from DB33/T 1191-2020 and Yong DX/JS 021-2023 (durations: 5–180 min; return periods: 1–100 yr)

IDF curves in this study

County	IDF Curves (Rainstorm Intensity Formula)	Data Period & Duration	Selection Method /Theoretical Distribution	Station and level
Area	(q, Rainstorm intensity (L/(s·hm ²)); t, Rainfall duration (min); P, Return period (years); lg, Common logarithm (base 10))		each duration / Gumbel	Basic • Update: 1980–2024 (45 years). • Annual maximum rainfall series for each duration. • Exponential
Beilun	$q = \frac{2664.628 \times (1 + 0.945 \lg P)}{(t + 13.262)^{0.763}}$	1980–2014 (35 years)		Beilun National General
Zhenhai	$q = \frac{2710.303 \times (1 + 0.958 \lg P)}{(t + 15.050)^{0.769}}$	1980–2014 (35 years)		Zhenhai National General
Fenghua	$q = \frac{799.935 \times (1 + 0.750 \lg P)}{(t + 2.080)^{0.508}}$	1980–2014 (35 years)		Fenghua National General
Xiangshan	$q = \frac{1311.955 \times (1 + 0.698 \lg P)}{(t + 6.741)^{0.575}}$	1980–2014 (35 years)		Xiangshan National General
Ninghai	$q = \frac{1287.699 \times (1 + 0.724 \lg P)}{(t + 4.676)^{0.579}}$	1980–2014 (35 years)		Ninghai National General
Yuyao	$q = \frac{2293.666 \times (1 + 0.698 \lg P)}{(t + 9.770)^{0.723}}$	1980–2014 (35 years)		Yuyao National General
Cixi	$q = \frac{3075.584 \times (1 + 0.854 \lg P)}{(t + 14.466)^{0.781}}$	1980–2014 (35 years)		Cixi National Basic



2.3.2 Extraction of typical spatiotemporal characteristics of typhoon rainfall

215 The 24-h rainfall processes corresponding to the values in the curve-fitting sequences of all stations were selected as the analysis samples. Based on the temporal distribution characteristics of these processes, the K-means method was used to classify them into different temporal rainfall patterns. For the processes within each type, weighted rainfall values were calculated for each time step of the specific duration. The weights were assigned according to the actual rainfall at the corresponding time step in the processes. The weighted values for all time steps within the specific duration were then normalized to obtain temporal allocation weights.

220 Subsequently, gridded data covering the Ningbo region (Fig. 1c) and corresponding to the time ranges of the selected processes were extracted. According to the spatial distribution characteristics of the gridded data for each rainfall process, K-means clustering was performed again. For the processes with the same spatial type, weighted cumulative rainfall for each grid over the specific duration was computed, with weights assigned according to the actual cumulative rainfall at each grid in the processes. These weighted values were then normalized to obtain spatial allocation weights.

225 Temporal rainfall patterns were identified using two key indicators: the position of the rainfall peak and the precipitation proportions in three intervals divided equally. For spatial patterns, the classification indices were defined as follows. First, the location of the main rainfall area was considered. The average position of the grids whose process-total rainfall was within the top 30% of all grids within a given duration was computed, and its distance from the regional centre was taken as the first index. The location of the target point relative to the regional centre was represented by two indices: its east–west
230 and north–south orientations. Next, the spatial distribution of the rainfall was examined, with focus on the dispersion of regions of high rainfall and the spatial gradient of precipitation. Four indices were calculated: the distance between the centroids of the top 30% and top 5% of grids ranked by process-total rainfall, the distance between the centroids of the bottom 30% and top 5% of grids ranked by process-total rainfall, the regional contribution ratio of process-total rainfall from the top 30% of grids, and the corresponding ratio for the bottom 30% of grids.

235 3 Results and discussion

3.1 Fitting results of IDF curves for typhoon rainfall

In this study, two sets of IDF curve fitting were conducted. The first was performed for the period 1980–2014, consistent with the data coverage of the existing IDF curves, which were developed in 2015 and remain in current use. This period was selected because both the quantity and the quality of rainfall data have increased substantially since 1980. Additionally, the
240 existing IDF curves were derived using precipitation data up to 2014, based on the local practical conditions and demands at that time. This fitting allowed comparative analysis highlighting the differences in rainfall intensity characteristics between curves with and without rainfall type distinction for the same period (1980–2014). The second fitting utilized more



comprehensive rainfall data from 1980–2024, with the specific objective of deriving IDF curves for typhoons that met current conditions and requirements.

245 Curve fitting performed best when using the Exponential distribution combined with the minimum sum of squared deviations criterion (Fig. 3). The fitted C_s/C_v ratios generally fall within the range of 2.5–4.0, concentrated predominantly between 3.0 and 3.5. These results are reasonable compared with the fixed values of C_s/C_v adopted in previous studies (Yu et al., 2021). Given the varied characteristics among different typhoons and the notable interannual differences in frequency, validation based on absolute error was found more suitable for assessing the results of this study. The RMSE of all curve fitting results was <0.06 mm/min, meeting standard accuracy requirements.

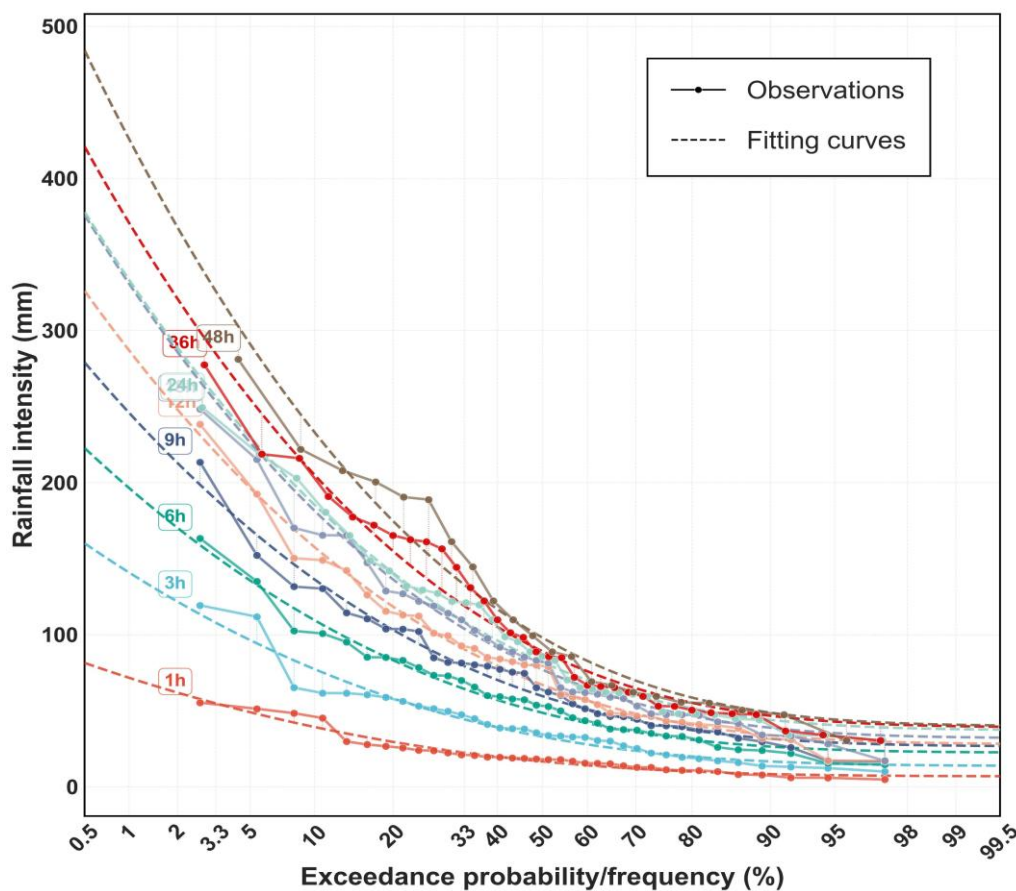


Figure 3: IDF curves for Yinzhou station (1980–2024) by duration. Solid lines represent observed results and dashed lines represent exponential fitting results, with different colours indicating different durations. Points on the two lines indicate rainfall intensity (mm) corresponding to specific return periods.

255 Taking Yinzhou station as an example, the intensity–frequency curves of typhoon, non-typhoon, and complete rainfall data at 1, 6, 12, and 24 h are compared in Fig. 4. For non-typhoon rainfall data and complete rainfall data, the rainfall process is considered to have ended when a period of at least 24 consecutive hours without precipitation occurs thereafter. When the green line lies above the blue line, this indicates that typhoons are more likely to produce rainfall of a given intensity and



that, for the same exceedance probability, they can generate more intense extreme rainfall. Comparison of the four subplots clearly shows that the blue and green curves begin to intersect at duration of 6 h and longer (Figs. 4b–d). As duration increases, the intersection position gradually moves towards the location of higher probability (Figs. 4c and d), indicating that the statistical characteristics of extreme rainfall exhibit clear dependence on duration and weather system. For short-duration extreme precipitation (e.g., 1 h), non-typhoon systems (such as the Meiyu front or severe convective weather) exhibit greater hazard potential (Fig. 4a). For long-duration extreme precipitation (e.g., 12 and 24 h; Fig. 4c and Fig. 4d, respectively), the rainfall intensity induced by typhoons can more readily reach or even exceed the levels associated with non-typhoon scenarios. This confirms quantitatively that typhoon systems are a key risk source for extreme precipitation under low frequency and long duration (e.g., those with a 100-year return period). The longer the duration, the greater the contribution of typhoons becomes to the statistical characteristics of extreme rainfall (Figs. 4b–d). Compared with non-typhoon convective systems with shorter lifespans and smaller spatial scales, the vast and more persistent rotational structure of typhoons enables them to sustain highly efficient moisture transport and convergent uplift over extended periods, thereby achieving substantial advantage in generating extreme accumulated rainfall.

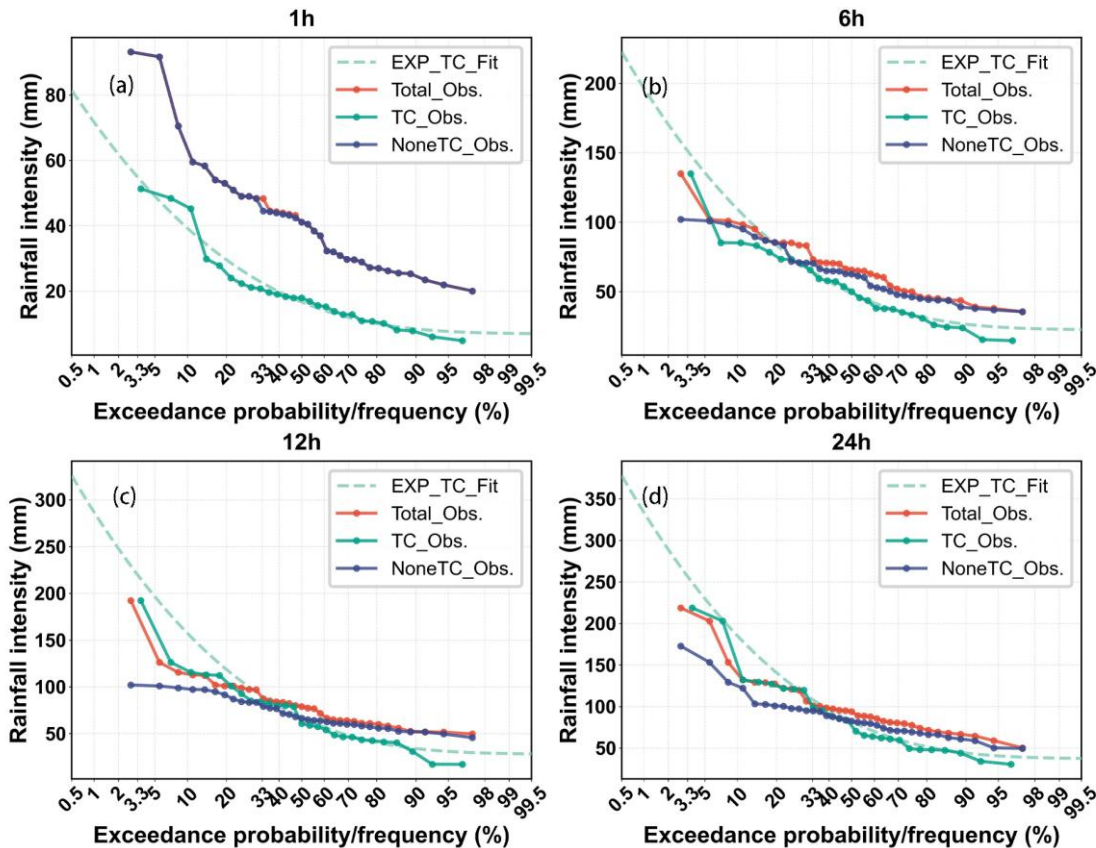
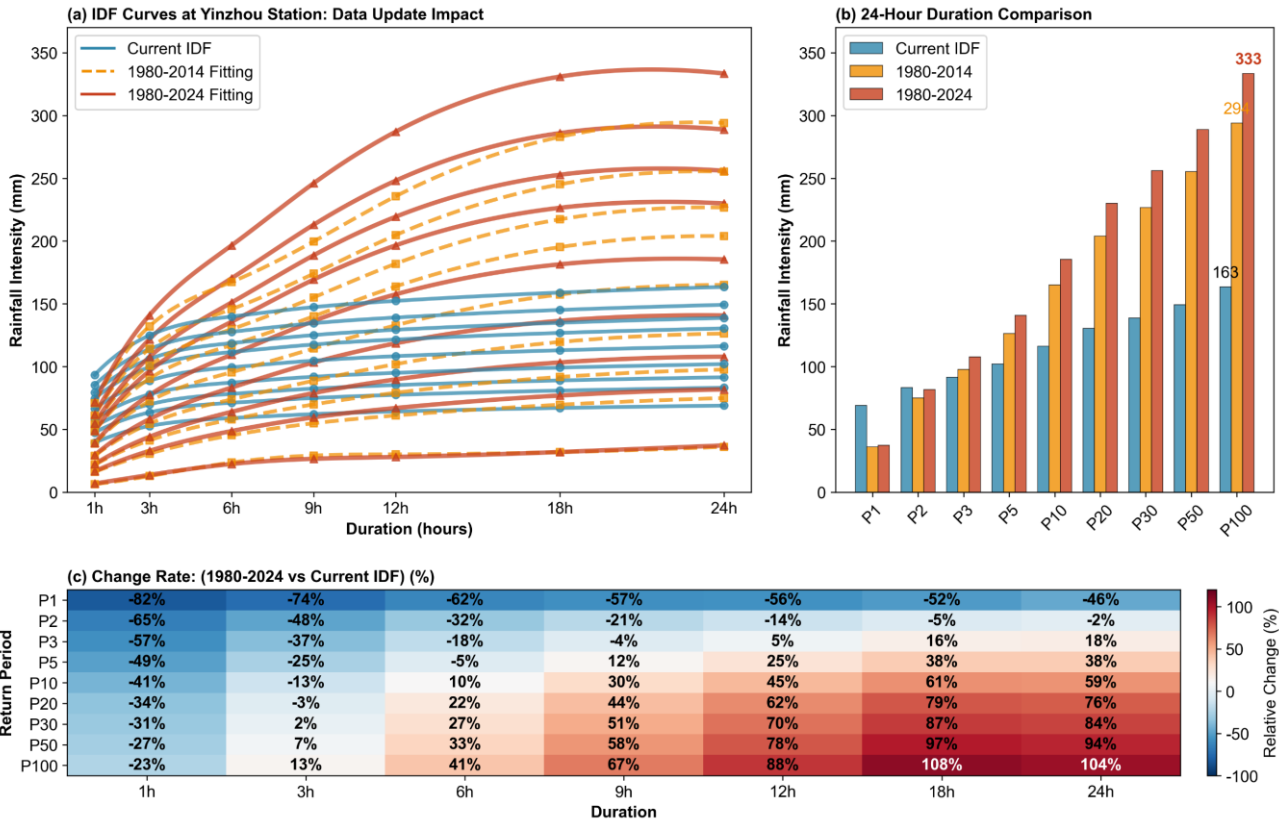


Figure 4: Annual maximum rainfall intensity–probability curves for Yinzhou Station during 1980–2014: (a) 1 h, (b) 6 h, (c) 12 h, and (d) 24 h, showing empirical probability points with connecting lines for complete (red), non-typhoon (blue), and typhoon (green) rainfall data, together with fitted intensity–frequency curves for typhoon rainfall (light green).



This study compared the fitted results with the currently published IDF curves. Intensities of typhoon rainfall at specific return periods are generally lower than those from the published IDF curves for short durations, but markedly higher for long durations, particularly for events with duration exceeding 6 h (Fig. 5a). Moreover, the differences are more pronounced for long durations after the data update (Fig. 5a). This reflects an essential difference in the dominant weather systems and physical mechanisms responsible for extreme rainfall across different durations. It is necessary to distinguish rainfall types (e.g., typhoon-type versus general-type) for differentiated design. The variation in intensity of typhoon rainfall with duration is more notable compared with the current IDF curves, and tends to stabilize after the 24-h processes (Fig. 5a). The newly developed curves reflect the unique characteristics of typhoons, exhibiting greater randomness and uncertainty. The primary hazard period is concentrated within 24 h, after which rainfall enters a phase of attenuation or stabilization. The applicability of the published IDF curves for extrapolating long-duration extreme rainfall intensities is limited (Fig. 5b). Designing based solely on the current IDF curves might result in insufficient drainage capacity for long-duration events. For urban drainage design, the intensity of typhoon rainfall within the 24-h window is a critical control target. Additionally, the hourly rainfall intensities produced by typhoons under high return periods remain comparable to the values of the published IDF curves at medium return periods (Fig. 5a). The non-typhoon weather systems make a greater contribution to extreme precipitation on the hourly scale, while typhoons, although responsible for a lesser contribution, remain capable of generating substantial hourly intensities. Extreme precipitation at longer durations (e.g., 24 h) driven by typhoon systems is characterized by higher accumulated rainfall rather than by instantaneous peak intensities of short-duration processes of convective weather systems (Fig. 5b). Comparison of the fitted results from different time periods shows that the rainfall intensities derived from the 1980–2024 series are markedly higher than those obtained from the 1980–2014 series, with greater increase observed for longer durations compared with shorter ones (Fig. 5a). This indicates that the impact of typhoon precipitation has continued to intensify in recent years. Under the current changing conditions, precipitation with high intensity and long duration that was previously less common is now more likely to occur (Fig. 5c). However, as indicated by the fitted data, this trend reflects an increase in the occurrence probability of such events, rather than a change in their extreme intensity.



300

Figure 5: Comparison of fitted results and currently published IDF curves. (a) Impact of data update on IDF curves: solid blue line represents the currently published IDF curves, dashed orange line represents the fitting curve for 1980–2014, and solid red line represents the fitting curve for 1980–2024. (b) Comparison of 24-h duration: blue bars represent the currently published IDF curves, orange bars represent the fitting curve for 1980–2014, and red bars represent the fitting curve for 1980–2024. (c) Change rate from the latest IDF curves to the currently published curves.

305

Marked regional spatial variations are observed across county-level areas. As a representative coastal station, Beilun station exhibits distinct characteristics of typhoon precipitation. The intensities of the fitting results all show high consistency with those obtained from the published IDF curves under high return periods (Fig. 6a). For this region, typhoons not only are the primary cause of high-impact extreme precipitation with long duration but also possess extreme hazard potential on short-
 310 duration scales, which is comparable to that of non-typhoon weather systems. Compared with Yinzhou station, Beilun station experiences considerably higher rainfall intensities. This phenomenon is related to its geographic location, which is more directly exposed to typhoons. The intensity at stations such as Fenghua and Ninghai is notably higher than that at Yinzhou station (table omitted). This difference is attributed primarily to the amplification effect of complex terrain on typhoon precipitation. Additionally, comparison of fitting results based on two time periods, i.e., 1980–2014 and 1980–2024,
 315 across various stations reveals that extending the observation series generally leads to increase in typhoon rainfall intensity for the same duration and return period. This trend is most pronounced for Yuyao station and Cixi station, both located in northern Ningbo, as illustrated by Yuyao station (Fig. 6b). Statistics further show that the increase in rainfall intensity is



driven primarily by a higher frequency of extreme precipitation rather than the surpassing of historical rainfall maxima. Under changing conditions, extreme precipitation from typhoons is transitioning from a “rare anomaly” into a “more frequent and high-risk phenomenon,” and thereby giving rise to new challenges for existing flood control and drainage systems.

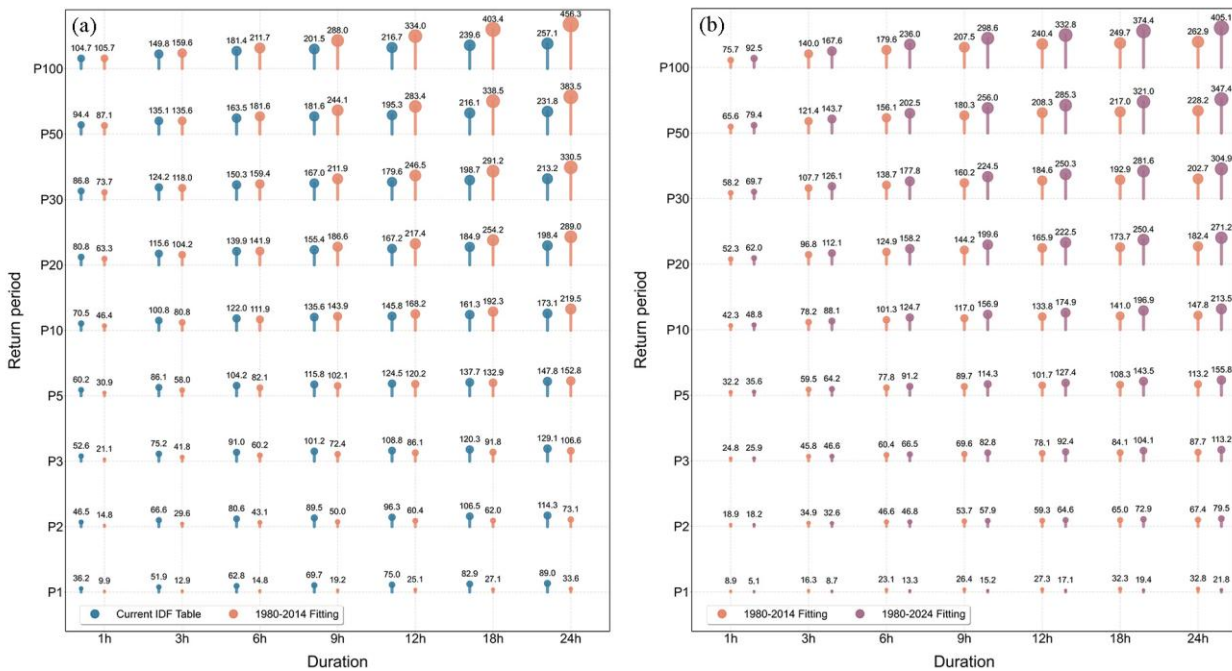
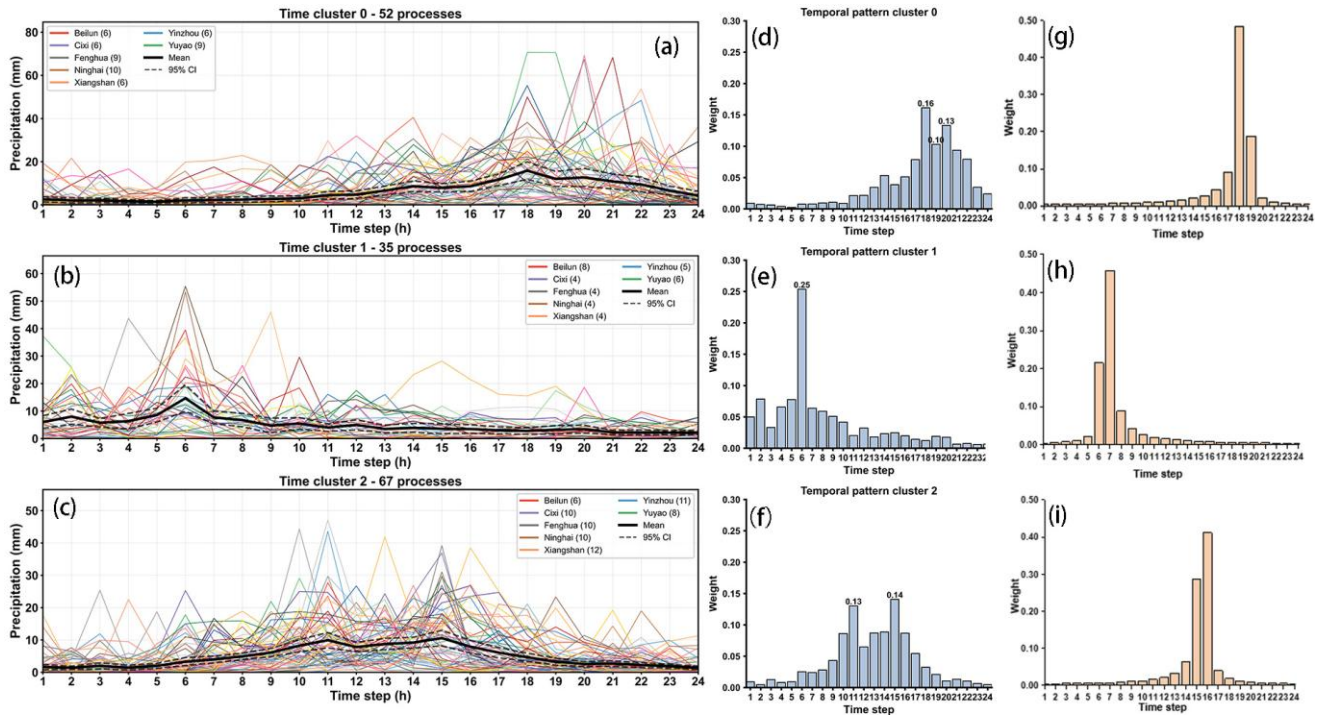


Figure 6: Rainfall intensities for various durations and return periods. (a) Beilun station: published sources (blue lollipops) and fitting results for 1980–2014 (orange lollipops) and (b) Yuyao station: fitting results for 1980–2014 (orange lollipops) and 1980–2024 (purple lollipops).

3.2 Analysis of spatiotemporal patterns of typhoon rainfall

The contribution of typhoons to extreme rainfall increases considerably with longer duration, and this characteristic is universal. The more severe impacts of extreme typhoon rainfall on the coastal and mountainous areas of the study region suggest that the recent increase in typhoon impacts is characterized by notable spatial non-uniformity. Additionally, thorough analysis of how these extreme 24-h rainfall records are realized through specific typhoon precipitation processes, including their spatiotemporal patterns, is crucial for rational design of drainage systems, reservoir operation strategies, and effective emergency management. Based on these findings, this study systematically extracted the key spatial and temporal patterns of rainfall by examining representative historical typhoon rainfall processes. Gridded data are available only from 1998 onward; therefore, to ensure consistency in the analysis of temporal and spatial patterns of rainfall, both analyses were based on station and gridded data from 1998 onwards.



340 **Figure 7: (a–c) Temporal classification of typical 24-h typhoon rainfall processes, with rainfall processes extracted from different stations marked in different colours. Typical 24-h rainfall temporal patterns in Ningbo City (blue bars): (d) late-peaked pattern, (e) early-peaked pattern, and (f) central-peaked pattern. Chicago hyetograph under different rainfall peak coefficients for a 100-year return period (orange bars): $r = 0.79$ (g), $r = 0.24$ (h), and $r = 0.51$ (i).**

The rainfall processes underlying the annual maximum 24-h rainfall sequences used for curve fitting at meteorological stations across Ningbo were extracted, and three distinct temporal patterns (Figs. 7d–f) were identified among the clustered rainfall processes (Figs. 7a–c). The proportions of the rainfall processes in the three categories were 33.77%, 22.73%, and 43.51%; the corresponding mean peak rainfall coefficients were 0.79, 0.24, and 0.51, while the mean proportions of rainfall during the marked rainfall phase were 60.69%, 56.09%, and 62.69%. All differences in these indicators between categories were statistically significant. Temporal rainfall patterns in Ningbo are characterized primarily by the late-peaked pattern (Fig. 7d) and the central-peaked pattern (Fig. 7f). The late-peaked pattern and the early-peaked pattern (Fig. 7e) exhibit relatively typical single-peak structures, with rainfall being more concentrated and hourly rainfall intensity displaying a relatively abrupt pattern. The central-peaked pattern (Fig. 7f) is more uniform and moderate, featuring a double-peak structure.

Using the current published IDF curves for Yinzhou station and the Chicago hyetograph method, the 24-h rainfall series at 5-min intervals was calculated. The rainfall peak coefficients for Ningbo, corresponding to Figs. 7d–f, were also applied, with the return period set to 100 years. Subsequently, the hourly rainfall pattern structure was derived by accumulating rainfall over 12 consecutive 5-min intervals. It can be observed that the rainfall distribution in the Chicago hyetograph is excessively



concentrated within a very short period, with the proportion of rainfall during the peak period exceeding 0.4 (Figs. 7g–i). In contrast, typhoon rainfall patterns show more moderate hourly intensity and gradient variations, differing considerably from the patterns generated by the Chicago hyetograph method. Therefore, it is recommended that the Chicago hyetograph not be applied directly as the temporal rainfall pattern for long-duration rainfall processes.

360

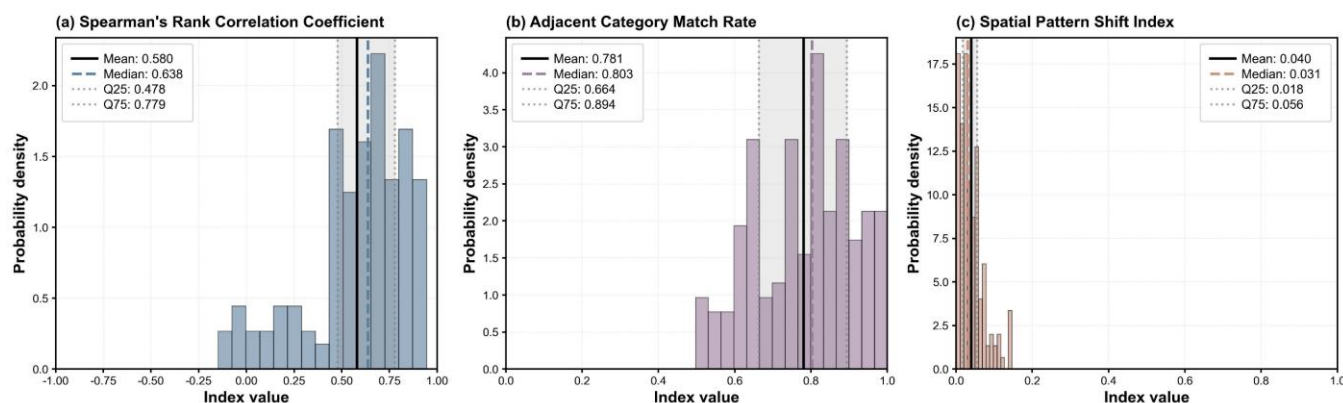


Figure 8: Comparison of gridded data and station data for the spatial distribution of representative 24-h typhoon rainfall processes. Indicators to characterize spatial inconsistency: (a) Spearman's rank correlation coefficient (blue bars), (b) adjacent category match rate (purple bars), and (c) spatial pattern shift index (orange bars).

365 The spatial distribution of rainfall varies among typhoon events in Ningbo. The spatial grid is densely distributed, enabling a more detailed description of the spatial distribution structure of each rainfall event compared with data from the sparse meteorological stations. Consequently, rainfall data for the grids corresponding to the occurrence time of the targeted 24-h events were extracted to facilitate a more refined and realistic spatial rainfall pattern analysis. The accuracy of gridded data must be verified. It is also important to note that this accuracy refers to how closely the spatial structure of the rainfall is represented by the gridded data compared with station data, not as a comparison of specific rainfall amounts. The consistency between the two types of data was assessed using three indices. First, the Spearman's rank correlation coefficient was employed to examine their monotonic relationship (Fig. 8a). Second, rainfall intensities from both datasets were ranked and grouped into five equal percentiles (quintiles), and the adjacent percentile matching rate was calculated as the proportion of grids with a percentile difference of ≤ 1 (Fig. 8b). Third, a spatial pattern shift index was constructed using rainfall magnitude-based weights to quantify the normalized displacement of rainfall centres between the two datasets (Fig. 8c). All three metrics consistently showed that the gridded data reliably captured the spatial rainfall distributions reflected by the station observations.

370 The processes under each temporal category were further divided into two subcategories according to the position of the areas of heavy rainfall and the spatial dispersion characteristics of the precipitation. The statistical significance tests under each temporal pattern indicated marked differences in the structural indices between the two spatial rainfall patterns. The first spatial rainfall pattern corresponding to the late-peaked temporal pattern exhibits a relatively uniform overall

380



distribution, with centres of heavy rainfall scattered in mountainous areas (Fig. 1b) and a relatively gentle north–south rainfall gradient (Fig. 9a). This category accounts for a relatively high proportion, reaching 73.08%. The second category is characterized by concentrated rainfall, with localized centres of heavy rainfall that account for a large proportion of the total regional rainfall. This pattern also displays a markedly pronounced northward offset (Fig. 9b). Between the two spatial rainfall patterns corresponding to the late-peaked temporal pattern, the first one is more dominant, accounting for 57.14%. It is characterized by a relatively uniform overall rainfall distribution, with scattered centres of heavy rainfall located primarily in southern mountainous areas (Fig. 1b), and exhibits a relatively high north–south rainfall gradient (Fig. 9c). The second one features concentrated precipitation, with extremely localized centres of heavy rainfall that account for a notably large proportion of the total regional rainfall (Fig. 9d). For the final two spatial rainfall patterns, the first pattern comprises 44 processes, representing the highest count among all spatial categories but accounting for a slightly lower proportion of 65.67%. This pattern is characterized by centres of heavy rainfall over northern mountainous areas, accompanied by extensive spatial coverage of precipitation (Fig. 9e). The second pattern features rainfall distributed primarily along the eastern coastal region of Ningbo (Fig. 9f), with notable longitudinal offset.

395

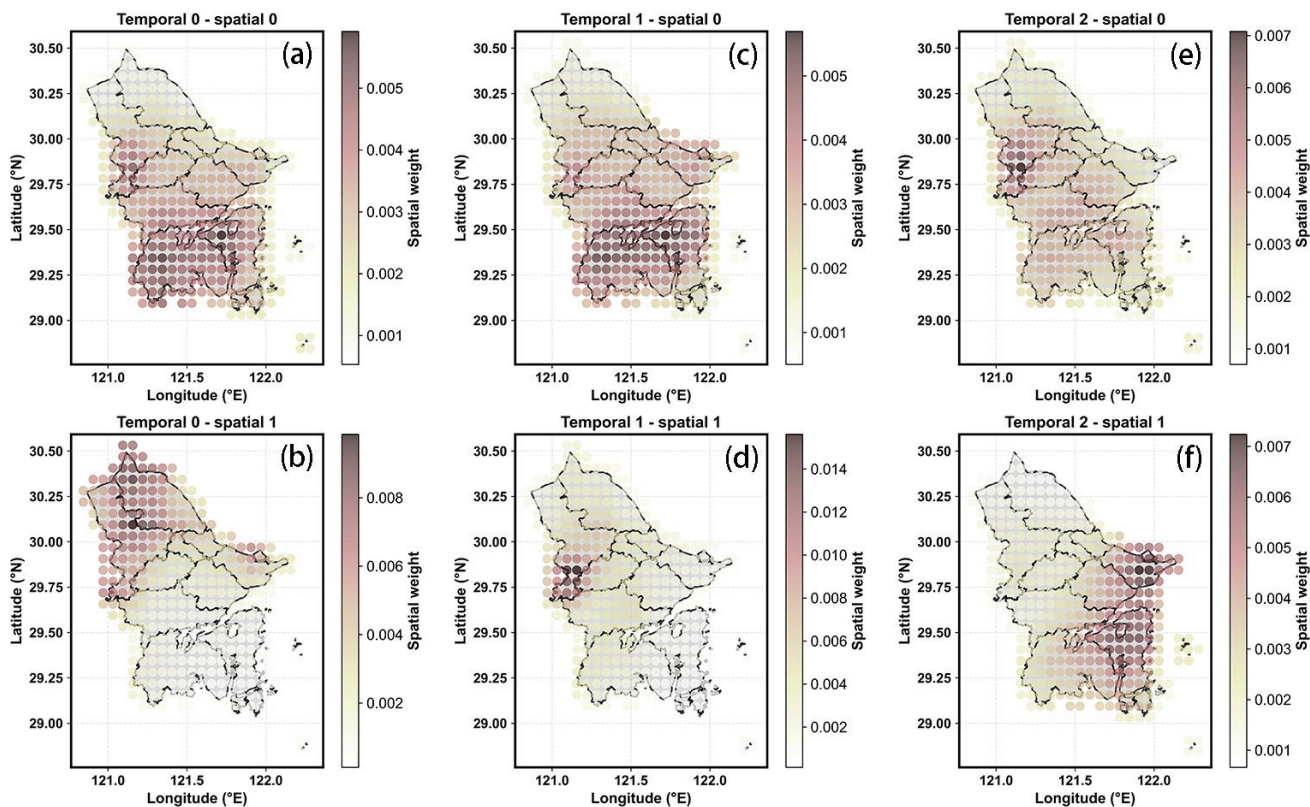


Figure 9: The three temporal rainfall patterns (late-peaked, early-peaked, and central-peaked), each with two spatial subtypes: (a, c, e) dispersed and (b, d, f) concentrated.



Overall, the spatial rainfall patterns can be summarized into the following two types. The first type can be described as the dispersed type, which predominates among the observed cases (Figs. 9a, c and e). This type is characterized by widespread rainfall coverage, with relatively scattered areas of heavy precipitation. The areas of maximum rainfall are typically distributed in high-elevation mountainous regions, and the regional rainfall gradient is relatively gentle. The second type can be considered the concentrated type (Figs. 9b, d and f). This type is distinguished by its compact areas of rainfall that account for a substantial proportion of the region's total precipitation. It often exhibits a notable longitudinal or latitudinal asymmetric distribution. The formation of this type is more complex, potentially influenced by inherent characteristics such as typhoon track movement (Fig. 8), or interactions between typhoons and other weather systems (e.g., westerly troughs, subtropical highs, and shear lines). This can be attributed to exceptionally abundant or sustained moisture transport, or to convergence, resulting in stronger localized impacts.

Analysis of the spatial and temporal patterns of typhoon rainfall reveals that factors such as typhoon track movement and underlying surface characteristics play important roles. Statistical analysis reveals that typhoon track often influences the extent of rainfall. For example, Figs. 9(b, d and e) shows typhoons with tracks shifted northward, while Fig. 9f reflects tracks distributed primarily east of the study region or along the eastern coast. The counterclockwise circulation of a typhoon shapes its asymmetric moisture transport, which is typically strongest on the eastern and southern sides. As this warm, moist airflow, driven by the Coriolis force and pressure gradients, moves towards land, it interacts dynamically with complex underlying terrain. In areas with trumpet-shaped topography, pronounced windward slopes, or curved coasts, the airflow is forced to converge and ascend, greatly enhancing local updrafts and precipitation efficiency, thereby shaping the final distribution of the centres of heavy rainfall (Figs. 9a, c and e). Rainfall in mountainous areas can sometimes intensify abruptly. Under typhoon conditions, the dynamic forcing of terrain on airflow can rapidly trigger or enhance convection within a short period. Additionally, the complex thermal properties of the underlying surface in mountainous regions tend to accumulate unstable energy locally, which can be released abruptly. These conditions might cause rainfall intensity to increase sharply over time (Figs. 7d and e) and exhibit localized intensification spatially (Figs. 9b and d). Unlike mountainous regions where topography plays a dominant role, over the northern plains and other gently sloping areas, the occurrence of widespread heavy rainfall induced by typhoons often requires effective dynamic and thermal coordination with other large-scale weather systems, such as westerly troughs and shear lines (Fig. 9b).

4 Summary and outlook

Traditional urban flood defence designs fail to consider the spatiotemporal non-uniformity of typhoon rainfall because they are based on classic rainfall patterns. This study took Ningbo in China as a case study. It established county-level IDF curves for annual maximum typhoon rainfall at specific durations using meteorological station observations. The K-means clustering method was then applied to extract typical spatiotemporal patterns of typhoon rainfall. The following three conclusions were derived.



The dominant role of typhoons in long-duration IDF relationships highlights the fundamental difference in their disaster-causing mechanisms compared with short-duration convective rainfall: the former triggers persistent urban flooding through cumulative rainfall, while the latter overwhelms the drainage system's instantaneous capacity with its peak intensity. Therefore, drainage and flood prevention design in typhoon-affected areas should account for the cumulative effects of long-
435 duration rainfall and establish categorized IDF curves and differentiated strategies. The current published IDF curves underestimate extremes for such prolonged processes. Moreover, in recent years, heavy typhoon-related rainfall of long duration has shown a notable trend of increase, particularly in the north of the study region.

Typhoon rainfall processes have predominantly exhibited late-peaked and central-peaked temporal patterns. The profiles differ substantially from the single-peak Chicago hyetograph, making the latter unsuitable for directly simulating long-
440 duration typhoon rainfall processes. Spatially, typhoon rainfall exhibits high inconsistency. The spatial structure of typhoon rainfall could be systematically categorized into two dominant types: dispersed and concentrated. The dispersed type corresponded to a relatively high proportion of samples and was characterized by extensive rainfall regions, scattered centres, and moderate gradients. Localized rainfall extent, asymmetric distribution, and concentrated intensity were the main features of the concentrated type of rainfall.

445 The dispersed type exhibited notable dependence on terrain, where topography might have also induced sudden intensification of rainfall over time. The concentrated type represented the primary mechanism for typhoon-induced regional localized extreme rainfall events, with more complex causation. Factors such as typhoon track and interactions with other weather systems regulated moisture transport and convergence processes, resulting in stronger spatial clustering of these rainfall types.

450 These findings provide a scientific basis for enhancing climate resilience and improving disaster prevention capabilities in coastal cities. However, to simplify the analysis of the spatial rainfall patterns, it was assumed that the spatial patterns remained generally unchanged over time. In realistic scenarios, typhoon rainbands might evolve or remain relatively stable over time. Meng et al. (2025) indicated that the movement of centres of rainfall can also influence the spatial distribution of flooding. Current discussions on the factors influencing spatial rainfall patterns rely primarily on qualitative analyses based
455 on regional characteristics. Future studies should further incorporate relevant influencing factors to conduct quantitative analyses and deepen the understanding of this issue.

Data availability

The best-track dataset for typhoons can be obtained from the official website of the Shanghai Typhoon Institute of the China Meteorological Administration (CMA) at <http://tcdata.typhoon.org.cn> (last access: 2 April 2025). Due to legal restrictions,
460 the hourly precipitation data used in this study cannot be publicly shared. For access requests, please visit the official website of the National Meteorological Information Center of the CMA at <https://data.cma.cn>. FABDEM data is freely available for download via the <https://doi.org/10.5523/bris.25wfy0f9ukoge2gs7a5mqpq2j7>.



Author contributions

CW contributed to data curation, the original draft preparation and editing of the manuscript, as well as methodology
465 development, and validation. YL participated in methodology refinement, reviewing and editing the manuscript, and
visualization, and initiated the projects which supported this work. HR contributed to the development of the research
methodology and reviewed and edited the manuscript. FR contributed to manuscript review and editing, funding acquisition,
project administration, and resource provision.

Competing interests

470 The contact author has declared that none of the authors has any competing interests.

Disclaimer

Copernicus Publications adds a standard disclaimer: “Copernicus Publications remains neutral with regard to jurisdictional
claims made in the text, published maps, institutional affiliations, or any other geographical representation in this paper.
While Copernicus Publications makes every effort to include appropriate place names, the final responsibility lies with the
475 authors. Views expressed in the text are those of the authors and do not necessarily reflect the views of the publisher.”
Please feel free to add disclaimer text at your choice, if applicable.

Acknowledgements

We thank editor and reviewers for helping us improving the clarity of the paper. YL was supported by Typhoon Scientific
and Technological Innovation Group of China Meteorological Administration CMA2023ZD06, FR was supported by the
480 Key Laboratory of South China Sea Meteorological Disaster Prevention and Mitigation of Hainan Province (SCSF202307),
the National Natural Scientific Foundation of China (42275037), and the Basic Research Fund of CAMS (2023Z016).

Financial support

This study was supported by Typhoon Scientific and Technological Innovation Group of China Meteorological
Administration CMA2023ZD06, the Key Laboratory of South China Sea Meteorological Disaster Prevention and Mitigation
485 of Hainan Province (SCSF202307), the National Natural Scientific Foundation of China (42275037), and the Basic Research
Fund of CAMS (2023Z016).



References

- Cannon, A. J. and Innocenti, S.: Projected intensification of sub-daily and daily rainfall extremes in convection-permitting climate model simulations over North America: implications for future intensity–duration–frequency curves, *Nat. Hazards Earth Syst. Sci.*, 19, 421–440, <https://doi.org/10.5194/nhess-19-421-2019>, 2019.
- 490 Chan, F. K. S., Gu, X., Qi, Y., Thadani, D., Chen, Y. D., Lu, X., Li, L., Griffiths, J., Zhu, F., Li, J., and Chen, W. Y.: Lessons learnt from Typhoons Fitow and In-Fa: implications for improving urban flood resilience in Asian Coastal Cities, *Nat. Hazards*, 110, 2397–2404, <https://doi.org/10.1007/s11069-021-05030-y>, 2022.
- Chen, G., Hou, J., Wang, T., Lv, J., Jing, J., Ma, X., Yang, S., Deng, C., Ma, Y., and Ji, G.: The effect of spatial-temporal characteristics of rainfall on urban inundation processes, *Hydrological Processes*, 36, e14655, <https://doi.org/10.1002/hyp.14655>, 2022.
- 495 Costabile, P., Costanzo, C., Kalogiros, J., and Bellos, V.: Toward Street-Level Nowcasting of Flash Floods Impacts Based on HPC Hydrodynamic Modeling at the Watershed Scale and High-Resolution Weather Radar Data, *Water Resources Research*, 59, e2023WR034599, <http://doi.org/10.1029/2023wr034599>, 2023.
- 500 Emanuel, K.: Assessing the present and future probability of Hurricane Harvey’s rainfall, *Proc. Natl. Acad. Sci. U.S.A.*, 114, 12681–12684, <https://doi.org/10.1073/pnas.1716222114>, 2017.
- Ghanmi, H., Bargaoui, Z., and Mallet, C.: Estimation of intensity-duration-frequency relationships according to the property of scale invariance and regionalization analysis in a Mediterranean coastal area, *Journal of Hydrology*, 541, 38–49, <https://doi.org/10.1016/j.jhydrol.2016.07.002>, 2016.
- 505 Gruss, Ł., Willems, P., Tomczyk, P., Pollert Jr., J., Pollert Sr., J., Märtner, C., Czaban, S., and Wiatkowski, M.: Evaluation of the Dual Gamma Generalized Extreme Value distribution for flood events in Poland, *Hydrol. Earth Syst. Sci.*, 29, 5165–5184, <https://doi.org/10.5194/hess-29-5165-2025>, 2025.
- Hawker, L., Uhe, P., Paulo, L., Sosa, J., Savage, J., Sampson, C., and Neal, J.: A 30 m global map of elevation with forests and buildings removed, *Environmental Research Letters*, 17, 024016, <https://doi.org/10.1088/1748-9326/ac4d4f>, 2022.
- 510 Hoch, J., Probyn, I., Marra, F., Lucas, C., Savag, J., Win, O., Sampson, C., and Addor, N.: BURGER: A bottom up regionalization approach for global sub daily Intensity Duration Frequency data, *Water Resources Research*, 61, e2024WR039773, <https://doi.org/10.1029/2024WR039773>, 2025.
- Hosking, J. R. M.: L-Moments: Analysis and Estimation of Distributions Using Linear Combinations of Order Statistics, *Journal of the Royal Statistical Society: Series B (Methodological)*, 52, 105–124, <https://doi.org/10.1111/j.2517-6161.1990.tb01775.x>, 1990.
- 515 Jayaweera, L., Wasko, C., Nathan, R., Syktus, J., and Eccles, R.: Evaluation and projection of extreme rainfall from a large ensemble of high-resolution regional climate models in Australia, *Weather and Climate Extremes*, 50, 100818, <https://doi.org/10.1016/j.wace.2025.100818>, 2025.



- Ji, J., Wang, Y., Jiang, T., Zhai, J., Sang, W., and Wu, H.: Analysis of characteristics of heavy rainfall events induced by landfalling tropical cyclones in China from 1980 to 2020, *Water Resources and Hydropower Engineering*, <https://link.cnki.net/urlid/10.1746.tv.20250709.1244.002>, 2025.
- Kossin, J. P.: A global slowdown of tropical-cyclone translation speed, *Nature*, 558, 104–107, <https://doi.org/10.1038/s41586-018-0158-3>, 2018.
- Lanciotti, S., Ridolfi, E., Russo, F., and Napolitano, F.: Intensity-Duration-Frequency Curves in a Data-Rich Era: A Review, *Water*, 14, 3705, <https://doi.org/10.3390/w14223705>, 2022.
- Li, L. and Chakraborty, P.: Slower decay of landfalling hurricanes in a warming world, *Nature*, 587, 230–234, <https://doi.org/10.1038/s41586-020-2867-7>, 2020.
- Li, X., Hou, J., Wang, Z., Wang, T., Lv, J., and Li, D.: Numerical simulation of the influence of design rainstorm pattern on urban flood in narrow valley, *Engineering Journal of Wuhan University*, <https://link.cnki.net/urlid/42.1675.T.20240830.0937.002>, 2024 (in Chinese).
- Lima, C. H. R., Kwon, H. H., and Kim, J. Y.: A Bayesian beta distribution model for estimating rainfall IDF curves in a changing climate, *Journal of Hydrology*, 540, 744–756, <https://doi.org/10.1016/j.jhydrol.2016.06.062>, 2016.
- Lin, B., Bonnin, G. M., Martin, D., Parzybok, T. M., Yekta, M., and Riley, D.: Regional frequency studies of annual extreme precipitation in the United States based on regional L-moments analysis, in: *Proceedings of the World Environmental and Water Resources Congress*, New York, American Society of Civil Engineers, 1, 16, [https://doi.org/10.1061/40856\(200\)219](https://doi.org/10.1061/40856(200)219), 2006.
- Lin, R., Zheng, F., Ma, Y., Duan, H.-F., Chu, S., and Deng, Z.: Impact of Spatial Variation and Uncertainty of Rainfall Intensity on Urban Flooding Assessment, *Water Resources Management*, 36, 5655–5673, <https://doi.org/10.1007/s11269-022-03325-8>, 2022.
- Liu, L. and Wang, Y.: Trends in Landfalling Tropical Cyclone-Induced Precipitation over China, *Journal of Climate*, 33, 2223–2235, <https://doi.org/10.1175/JCLI-D-19-0693.1>, 2020.
- Lu, X., Yu, H., Ying, M., Zhao, B., Zhang, S., Lin, L., Bai, L., and Wan, R.: Western North Pacific tropical cyclone database created by the China Meteorological Administration, *Adv. Atmos. Sci.*, 38, 690–699, <https://doi.org/10.1007/s00376-020-0211-7>, 2021.
- Meng, D., Liao, Y., Deng, Z., Chen, Y., Lai, C., Chen, X., and Wang, Z.: Spatially moving non-uniform rainstorms may exacerbate urban flooding disasters, *Journal of Hydrology*, 660, 133374, <https://doi.org/10.1016/j.jhydrol.2025.133374>, 2025.
- Ministry of Land, Infrastructure, Transport and Tourism (MLIT), Water Management and National Land Protection Bureau: Methods for setting design maximum external forces for creating flood and internal water inundation assumptions[R], Tokyo: Ministry of Land, Infrastructure, Transport and Tourism., https://www.mlit.go.jp/river/shishin_guideline/pdf/shinsuisoutei_honnun_1507.pdf, 2015.



- Ministry of Land, Infrastructure, Transport and Tourism (MLIT), Water Management and National Land Protection Bureau, River Environment Department, Flood Control Planning Office and National Institute for Land and Infrastructure Management (NILIM), River Research Department, Flood Disaster Research Laboratory: Guidelines for the examination and creation of multi-stage flood inundation assumption maps and flood risk maps[R], Tokyo: Ministry of Land, Infrastructure, Transport and Tourism., https://www.mlit.go.jp/river/shishin_guideline/pdf/guideline_kouzuishinsui_2301.pdf, 2023.
- National Standardization Administration of China, General Administration of Quality Supervision, Inspection and Quarantine of the People's Republic of China: Grade of precipitation, GB/T 28592-2012, China Standard Press, Beijing, China, <https://openstd.samr.gov.cn/bzgk/gb>, 2012 (in Chinese).
- Ningbo Housing and Urban-Rural Development Bureau: Rules for Urban Flooding Prevention and Control in Ningbo, Yong DX/JS 021-2023, Ningbo, China, <http://zjw.ningbo.gov.cn>, 2023 (in Chinese).
- Qi, W., Ma, C., Xu, H., and Zhao, K.: Urban flood response analysis for designed rainstorms with different characteristics based on a tracer-aided modeling simulation, *J. Clean. Prod.*, 355, 131797, <http://doi.org/10.1016/j.jclepro.2022.131797>, 2022.
- Ren, Z., Sang, Y. F., Cui, P., Chen, F., and Chen, D.: A dataset of gridded precipitation intensity-duration-frequency curves in Qinghai-Tibet Plateau, *Scientific Data*, 12, 3, <https://doi.org/10.1038/s41597-024-04362-1>, 2025.
- SCS U: Urban hydrology for small watersheds, technical release no. 55 (TR-55), US Department of Agriculture, US Government Printing Office, Washington, DC, 1986.
- Sivapalan, M. and Blöschl, G.: Transformation of point rainfall to areal rainfall: Intensity-duration-frequency curves, *Journal of Hydrology*, 204, 150–167, [https://doi.org/10.1016/S0022-1694\(97\)00117-0](https://doi.org/10.1016/S0022-1694(97)00117-0), 1998.
- Su, Z., Ren, F., Wei, J., Lin, X., Shi, S., and Zhou, X.: Changes in Monsoon and Tropical Cyclone Extreme Precipitation in Southeast China from 1960 to 2012, *Trop. Cyclone Res. Rev.*, 4, 12–17, <https://doi.org/10.6057/2015TCRR01.02>, 2015.
- Sun, S., Shi, C., Pan, Y., Bai, L., Xu, B., Zhang, T., Han, S., and Jiang, L.: Applicability Assessment of the 1998–2018 CLDAS Multi-Source Precipitation Fusion Dataset over China, *J. Meteorol. Res.*, 34, 879–892, <https://doi.org/10.1007/s13351-020-9101-2>, 2020.
- Tang, Q., Bao, Y., Chen, C., Wang, T., Wu, J., Yu, T., and Zheng, X.: Spatio-temporal characteristics of rainstorm in Kunshan and reckoning of designed rainstorm intensity formula, *Journal of Tropical Meteorology*, 36, 683–698, <https://doi.org/10.16032/j.issn.1004-4965.2020.062>, 2020 (in Chinese).
- Wang, J., Li, S., Guan, X., He, Y., Cao, C., Lian, L., and Zhang, L.: Unveiling the Link Between Extreme Precipitation Events and Flood Disasters in China: From 3D Perspective, *EGUsphere [preprint]*, <https://doi.org/10.5194/egusphere-2025-4728>, 2025.
- Xu, H., Tian, Z., Sun, L., Ye, Q., Ragno, E., Bricker, J., Mao, G., Tan, J., Wang, J., Ke, Q., Wang, S., and Toumi, R.: Compound flood impact of water level and rainfall during tropical cyclone periods in a coastal city: the case of Shanghai, *Nat. Hazards Earth Syst. Sci.*, 22, 2347–2358, <https://doi.org/10.5194/nhess-22-2347-2022>, 2022.



- Xu, S., Wang, Q., Yu, J., Zhao, G., Ji, H., Yue, Q., Zheng, Y., Xu, H., Li, H., and Yao, X.: The impact of the spatiotemporal structure of rainfall on flood response over a piedmont urban basin: An approach coupling machine learning and hydrologic modeling, *Journal of Hydrology*, 659, 133160, <https://doi.org/10.1016/j.jhydrol.2025.133160>, 2025.
- 590 Yan, Z., Xia, J., Song, J., Zhao, L., and Pang, G.: Research progress on design hyetographs in small and medium-scale basins, *Progress in Geography*, 39, 1224–1235, <https://doi.org/10.18306/dlkxjz.2020.07.014>, 2020 (in Chinese).
- Yang, Z., Wang, J., Liu, J., Wang, H., Mei, C., and Li, F.: Construction of urban rainfall scenario database and matching technology for predicting rain fall, *Water Resources and Hydropower Engineering*, 55, 13–24, <https://doi.org/10.13928/j.cnki.wrahe.2024.10.002>, 2024 (in Chinese).
- 595 Ying, M., Zhang, W., Yu, H., Lu, X., Feng, J., Fan, Y., Zhu, Y., and Chen, D.: An overview of the China Meteorological Administration tropical cyclone database, *J. Atmos. Ocean. Tech.*, 31, 287–301, <https://doi.org/10.1175/JTECH-D-12-00119.1>, 2014.
- Yu, C., Xu, Q., Yang, Y., Ma, G., and Gao, X.: Intensity formula and design hyetograph for long-duration storm in Xiong’an New District, *Journal of Meteorology and Environment*, 37, 78–85, <https://doi.org/10.3969/j.issn.1673-503X.2021.05.012>, 2021 (in Chinese).
- 600 Zhang, M., Xu, M., Wang, Z., and Lai, C.: Assessment of the vulnerability of road networks to urban waterlogging based on a coupled hydrodynamic model, *Journal of Hydrology*, 603, 127105, <https://doi.org/10.1016/j.jhydrol.2021.127105>, 2021.
- Zhang, Q., Lai, Y., Gu, X., Shi, P., and Singh, V. P.: Tropical cyclonic rainfall in China: Changing properties, seasonality, and causes, *J. Geophys. Res.-Atmos.*, 123, 4476–4489, <https://doi.org/10.1029/2017JD028119>, 2018.
- 605 Zhang, X.: Study on the Characteristics of Summer Precipitation and Their Influence on Design Storm Parameters in the Beijing Area[D], Nanjing University of Information Science and Technology, 2015 (in Chinese).
- Zhao, Y., Zhang, Q., Ju, X., Xiao, D., Yang, H., Chen, J., Liao, J., and Deng, Y.: Analysis of the Characteristics of Short Term Extreme Precipitation in China in the Last 30 Years, *Chinese Journal of Atmospheric Sciences*, 48, 1144–1156, <https://doi.org/10.3878/j.issn.1006-9895.2212.22118>, 2024 (in Chinese).
- 610 Zhejiang Province Department of Housing and Urban-Rural Development: Standard of rainfall intensity computation, DB 33/T 1191–2020, Hangzhou, China, <http://zjw.ningbo.gov.cn>, 2020 (in Chinese).
- Zhou, C., Chen, P., Yang, S., Zheng, F., Yu, H., Tang, J., Lu, Y., Chen, G., Lu, X., Zhang, X., and Sun, J.: The impact of Typhoon Lekima (2019) on East China: a postevent survey in Wenzhou City and Taizhou City, *Front. Earth Sci.*, 16, 109–120, <https://doi.org/10.1007/s11707-020-0856-7>, 2022.